

Resistive-switching behavior in stacked graphene diode

Motoki Ohi^{1*}, Fumiya Fukunaga¹, Hayate Murakami¹, Hiroyuki Kageshima³,

Yasuhide Ohno^{1,2}, and Masao Nagase^{1,2*}

¹*Graduate school of Sciences and Technology for Innovation, Tokushima University, Japan*

²*Institute of Post-LED Photonics, Tokushima University, Japan*

³*Graduate School of Natural Science and Technology, Shimane University, Japan*

E-mail: m_ohi@ee.tokushima-u.ac.jp

In this study, stacked graphene diodes were fabricated via direct bonding using single-crystal graphene on a SiC substrate. Switching and S-shaped negative resistance were observed in the junction electrical properties measured via the 4-terminal configuration. The high-resistance state switched to the low-resistance state after applying a maximum junction voltage of ~ 10 V. In the high-bias voltage region, the junction voltage decreased from the maximum junction voltage to a few volts, indicating a negative resistance. In the high-resistance state, junction conductance was nearly constant at 0.13 mS. Electrical conductance in the high-bias region was expressed using an exponential function with an exponent of -1.26 . Therefore, the fabricated stacked graphene diode with a simple device structure demonstrated strong nonlinear electrical properties with negative differential conductance.

1. Introduction

Graphene, a two-dimensional material, has several unique properties, such as high carrier mobility and a peculiar band structure, and is expected to have applications across varied fields owing to its excellent electrical and mechanical properties¹⁻⁵). Recently, stacked graphene systems constructed using two individual graphene layers have attracted significant attention owing to their unique properties, such as superconductivity⁶, insulation^{7,8}, and band gap formation⁹⁻¹²). Stacked graphene diodes have also been reported to have specific electronic and optical properties¹³). Hence, various types of stacked graphene diodes have been fabricated, both with and without insulating materials between the layers. Further, nonlinear I - V characteristics were observed in tunneling diodes with insulating materials. The resonant tunneling phenomenon with negative differential conductance^{14,15}, terahertz emission¹⁶, and quantum point contacts^{17,18} was realized in the stacked graphene-insulator-graphene devices. Further, directly bonded graphene-graphene diodes typically have linear I - V characteristics¹⁹⁻²¹). Recently, N. Murakami et al. reported nonlinear I - V characteristics in stacked graphene far infrared emitter²²). However, the nonlinear electrical properties were not discussed in detail. Because graphene is semi-metal, a switching device with high on-off ratio has not been established. The nonlinear characteristics of the stacked graphene diode are expected to realize a switching device based on the new physical phenomenon.

In this study, the electrical properties of stacked graphene diodes fabricated using direct bonding techniques are discussed. Two graphene samples stacked face-to-face were epitaxially grown on 100 mm² SiC substrates via thermal decomposition. The large-area graphene samples enabled 4-terminal measurements, and the electrical properties of the graphene junctions were measured. Nonlinear electrical behavior was observed in these stacked graphene diodes. Additionally, S-shaped negative resistance was observed during 4-terminal measurement. The switching behavior from high- to low-resistance states was also observed through I - V characteristics and time-dependent measurements. Accordingly, the device parameters of the stacked graphene diodes were successfully extracted.

2. Experimental methods

2.1 Fabrication of epitaxial graphene samples

Graphene samples were prepared using an infrared rest heat annealing system (Thermo Riko SR-1800)²³). The initial material was a semi-insulating 4H-SiC (0001) substrate of area 100 mm². Six graphene samples were prepared for fabricating three stacked graphene diodes.

The annealing conditions for epitaxial graphene growth were 1630 °C for 5 min in a 100-torr Ar environment (see details in Supplementary Data). Micro-Raman spectroscopy and SPM results indicated that these samples were covered with high-quality single-crystal graphene films²³). The typical sheet resistance of the monolayer graphene samples was approximately 1079 Ω/sq , typical carrier mobility was approximately 1137 cm^2/Vs , and typical carrier (electron) density was approximately $5.4 \times 10^{12} \text{ cm}^{-2}$. High electron doping levels were the optimal condition for epitaxial graphene growth on SiC substrates^{23)–26}). This electron doping significantly lowered the metal contact resistance²⁷).

2.2 Fabrication of the stacked graphene diodes

Graphene junctions were fabricated by directly bonding two graphene samples grown as n-type monolayer graphene on the SiC substrate, as shown in Fig. 1. One sample was rotated 60° to align their crystallographic orientations and fixed with acrylic molds. Next, a gold-coated contact probe was placed at the four corners of each sample for 4-terminal measurement to confirm the electrical properties of the graphene junction. The typical load force of the contact probe was 0.27 N. Figure 1(c) shows a photograph of the stacked graphene diodes. The electrical properties of the three devices (Devices 1, 2, and 3) were measured using a semiconductor-device parameter analyzer (Keysight B1500A). All measurements were performed in air at room temperature.

3. Results and discussion

3.1 Evaluation of electrical properties

To evaluate the stacked graphene diodes, their electrical properties were measured over 2 and 4 terminals (Fig. 1(a)). Figure 2 shows the equivalent circuit of the stacked graphene diode, where V_b and V_j are the 2 and 4-terminal voltages of the stacked graphene diode, respectively. R_a is the access resistance comprising the contact (gold-coated electrodes and graphene) and parasitic resistances of the graphene film in the junction area. R_j is the graphene junction resistance measured via the 4-terminal configuration. The electrical properties of the devices, including all the resistive components, were measured using the 2-terminal configuration, and the electrical properties of the graphene junctions were measured using the 4-terminal configuration.

3.2 Current–voltage characteristic of stacked graphene diode

Figure 3 shows (a) 2-terminal $I-V_b$ characteristics of the device and (b) 4-terminal $I-V_j$ characteristics of the graphene junction (Device 1). Although graphene–metal and graphene–graphene contacts are generally ohmic, weak nonlinearities were observed, as shown in Fig.

3(a). In Fig. 3(b), the current (I) increased with 2-terminal voltage (V_b). The junction voltage (V_j) increased to 12 V with V_b in the low voltage applied region ($V_b < \sim 40$ V). In the high bias voltage applied region ($V_b > \sim 40$ V), V_j decreased from 12 V to 2.0 V, indicating negative resistance. The I - V characteristics of the negative bias region exhibited nearly identical behavior. The stacked graphene diode showed symmetric S-shaped I - V characteristics. The junction resistance (R_j) was high (5.9 k Ω) in the low bias voltage region and low (0.2 k Ω) in the high bias voltage region ($|V_b| = 90$ V). The on-off ratio of junction resistance for this device was approximately 30.

3.3 Time-dependent measurements of graphene-graphene junction

Figure 4 illustrates the time dependence $I(t)$ - $V_j(t)$ for various V_b . Plots of the initial state $I(0)$ - $V_j(0)$ show the ohmic characteristics with a resistance of 5.3 k Ω , which is similar to the junction resistance of the I - V characteristics. Furthermore, the plots of the final state ($t = 1500$ s) show similar characteristics as that of I - V_j in Fig. 3(b). These results indicate that the initial state (high resistance) transitioned to the final state (low resistance) upon the application of bias voltage. Figures 5 shows (a) V_j and (b) I at high ($V_b = 90$ V) and low ($V_b = 10$ V) voltages over time. At high bias voltage ($V_b = 90$ V), the initial voltage $V_j(0)$ and current $I(0)$ were 24 V and 4.1 mA, respectively. At $t = 1500$ s, V_j decreased to 2.2 V and I increased to 7.0 mA. Conversely, at low bias voltage ($V_b = 10$ V), $V_j(0)$ and $I(0)$ were 2.7 V and 0.5 mA, respectively. Both voltage and current have no time dependence in the low bias voltage region. Additionally, the low resistance states in the high bias voltage region immediately reset to high resistance when the bias voltage is set to zero.

3.4 Conductance-voltage characteristic of stacked graphene diode

Figure 6(a) shows the junction conductance (G_j)-voltage (V_j) characteristics of Device 2 fabricated with the other pair of graphene samples. G_j is given by

$$G_j = \frac{I}{V_j} \quad (1)$$

The inset shows the 4-terminal I - V_j characteristics of this device. The I - V_j characteristics in the inset of Fig. 6(a) are similar to those in Fig. 3(b) (Device 1). Its turn-on voltage of 7.65 V is lower than that of Device 1, as shown in Fig. 3(b). The on-off ratio of Device 2 is approximately 76, which is larger than that of Device 1. The I - V_j characteristics show complex behavior in the high bias region. The behavior of the I - V_j curve is difficult to express using a simple analytical function. Conversely, as shown in Fig. 6(a), the G_j - V_j curve linearly increases in the high-bias region. Figure 6(b) shows a double logarithmic graph of

the G_j - V_j curves for three different devices (Devices 1, 2, and 3). The graph shows the characteristics of the device. The conductance in the low-bias region G_{j0} was constant. The conductance in the high-bias region can be expressed via an exponential function as follows:

$$G_j = S_0 \cdot V_j^{-a} \quad (2)$$

where S_0 is a pre-factor and a is an exponent. In Table 1, the device parameters (on-off ratio, $|V_{j\text{-max}}|$, G_{j0} , S_0 , and a) of the three devices are summarized. Because the maximum current in the high-bias region (90 V) was primarily limited by the access resistance R_a , the resistance value in the low-resistance state was strongly affected by the contact resistance between the contact probe and graphene. The on-off ratio of the three devices ranged from 11.1 to 75.9. As shown in Table 1, $|V_{j\text{-max}}|$ ranged from 7.65 V to 12.7 V. Currently, the physical significance of the maximum junction voltage is unclear. The electrons with maximum junction voltage energy should be induced via inter band tunneling, namely π - π^* (4.7 eV@M) or σ - σ^* (14.6 eV@ Γ)²⁸. The high-energy ballistic electrons traveling between the two graphene layers may play an important role in the S-shaped I - V characteristics²⁹. These S-shaped characteristics of the graphene device are expected to be realized in terahertz applications because the negative differential conductance and high graphene mobility are suitable for a high-frequency oscillator. The average initial conductance (G_{j0}) was 0.13 mS. This conductance value was similar to the value of quantum conductance (0.08 mS). Because the graphene samples were slightly bent owing to high-temperature annealing, the effective junction area of the stacked graphene diode was smaller than the sample size. The estimated junction area using graphite c-axis resistivity ($\sim 3.34 \times 10^{-9} \Omega \text{ cm}^2$)^{30,31} was 43 nm², which is reasonable for quantum point contact. The exponent a in the device parameters, whose average value was 1.26, was identical for the three devices. The device parameter a indicates the physical characteristics of the three devices. As shown by the orange line in Fig. 6(b), G_j increases with the same slope for these devices. If G_j can be expressed as an exponential function of Eq. (2), dI/dV_j , which is generally related to the density of states of the band structure, can be expressed as the same exponential function. These results suggest that the S-shaped I - V characteristics of the stacked graphene diode originate from the graphene band structure. However, more detailed experiments and theoretical discussions are required to clarify the origin of negative conductance. To utilize the switching behavior and negative conductance in real applications, the access resistance, R_a , must be reduced to be below the low-resistance state. Fortunately, the contact resistivity between metal electrodes and

graphene on SiC is low²⁷). The reduction of R_a can be easily established by increasing of the area of contact electrodes. In the future, terahertz oscillator and emitter will be realized by using the stacked graphene diode.

4. Conclusions

In this study, stacked graphene diodes consisting of two epitaxial graphene layers were fabricated. A stacked graphene diode was constructed via simple direct bonding. Lithography was not employed for the fabrication of the graphene-graphene junction and metal electrodes. Using a 4-terminal configuration, the junction characteristics, except the parasitic resistance, were successfully measured. The junction resistance was switched from a high-resistance state to a low-resistance state by applying bias voltage. The maximum applied voltage (~ 10 V) induced an inter band tunneling between the two graphene layers, which is one possible cause for switching. The conductance value of the high-resistance state suggests that a point contact of nanometer size was formed at the bonding region of the two graphene layers. The negative resistance in the low-resistance region will be useful for oscillator applications in the terahertz frequency range. The stacked graphene diode with the sample structure is expected to facilitate next-generation electrical devices.

Acknowledgments

This work was supported by JSPS KAKENHI, Grant Numbers JP19H02582 and JP21H01394.

References

- 1) K. S. Novoselov, V. I. Fal'ko, L. Colombo, P. R. Gellert, M. G. Schwab, and K. Kim, *Nature* **490**, 192 (2012).
- 2) K. S. Novoselov, A. K. Geim, S. V. Morozov, D. Jiang, M. I. Katsnelson, I. V. Grigorieva, S. V. Dubonos, and A. A. Firsov, *Nature* **438**, 197 (2005).
- 3) K. S. Novoselov, A. K. Geim, S. V. Morozov, D. Jiang, Y. Zhang, S. V. Dubonos, I. V. Grigorieva, and A. A. Firsov, *Science* **306**, 666 (2004).
- 4) A. H. C. Neto, F. Guinea, N. M. R. Peres, K. S. Novoselov, and A. K. Geim, *Rev. Mod. Phys.* **81**, 109 (2009).
- 5) F. Memarian, A. Ffereidoon, M. D. Ganji, *Superlattices Microstruct.* **85**, 348 (2015).
- 6) Y. Cao, V. Fatemi, S. Fang, K. Watanabe, T. Taniguchi, E. Kaxiras, P. J. Herrero, *Nature*, **556**, 43 (2018).
- 7) A. L. Grushina, D. Ki, M. Koshino, A. A. L. Nicolet, C. Faugeras, E. McCann, M. Potemski, and A. F. Morpurgo, *Nat. Commun.* **6**, 6419 (2015).
- 8) Y. Cao, V. Fatemi, A. Demir, S. Fang, S. L. Tomarken, J. Y. Luo, J. D. S. Yamagishi, K. Watanabe, T. Taniguchi, E. Kaxiras, R. C. Ashoori, and P. J. Herrero, *Nature* **556**, 80 (2018).
- 9) Y. Zhang, T. Tang, C. Girit, Z. Hao, M. C. Martin, A. Zettl, M. F. Crommie, Y. R. Shen, and F. Wang, *Nature* **459**, 820 (2009).
- 10) H. Min, B. R. Sahu, S. K. Banerjee, A. H. MacDonald, *Phys Rev. B* **75**, 155115 (2007).
- 11) M. L. Ould NE, M. Boujnah, A. Beyoussef, A. El. Kenz, *J Supercond Nov Magn* **30**, 1263 (2017).
- 12) K. Sato, N. Hayashi, T. Ito, N. Masago, M. Takamura, M. Morimoto, T. Maekawa, D. Lee, K. Qiao, J. Kim, K. Nakagahara, K. Wakabayashi, H. Hibino, and W. Norimatsu, *Commun. Mater.* **2**, 117 (2021).
- 13) D. Yadav, S. B. Tombet, T. Watanabe, S. Arnold, V. Ryzhii, and T. Otsuji, *2D Mater.* **3** 045009 (2016).
- 14) L. Britnell, R. V. Gorbachev, A. K. Geim, L. A. Ponomarenko, A. Mishchenko, M. T. Greenaway, T. M. Fromhold, K. S. Novoselov, and L. Eaves, *Nat. Commun.* **4**, 1794 (2013).
- 15) A. Alzahrani, A. Alrqi, B. Karki, M. K. Koralalage, J. Jasinski, and G. Sumanasekera, *Nano Express* **2**, 040010 (2021).
- 16) D. Yadav, G. Tamamushi, T. Watanabe, J. Mitsushio, Youssef Tobah, K. Sugawara, A. A. Dubinov, A. Satoru, M. Ryzhii, V. Ryzhii and T. Otsuji, *J. Nanophotonics.*, **7**, 741 (2018).
- 17) D. Bischoff, M. Eich, O. Zilberberg, C. Rossler, T. Ihn, and K. Ensslin, *Nano Lett.* **15**, 6003 (2015).

- 18) H. Sadeghi, D. T. H. Lai, J. M. Redoute, and A. Zayegh, *J. Nanomater.* **2013**, 127690 (2013).
- 19) D. Chae, D. Zhang, X. Huang and K. V. Klitzing, *Nano. Lett* **12**, 3905 (2012).
- 20) Y. Kim, H. Yun, S. Nam, M. Son, D. S. Lee, D. C. Kim, S. Seo, H. C. Choi, H. Lee, and J. S. Kim, *Phys. Rev. Lett.* **110**, 096602 (2013).
- 21) J. Du, Y. Kimura, M. Tahara, K. Matsui, H. Teratani, Y. Ohno, and M. Nagase, *Jpn. J. Appl. Phys.* **58** SDDE01 (2019).
- 22) N. Murakami, Y. Sugiyama, Y. Ohno, and M. Nagase, *Jpn. J. Appl. Phys.* **60**, SCCD01 (2021).
- 23) T. Aritsuki, T. Nakashima, K. Kobayashi, Y. Ohno, and M. Nagase, *Jpn. J. Appl. Phys.* **55** 06GF03 (2016).
- 24) K. Kobayashi, S. Tanabe, T. Tao, T. Okumura, T. Nakamura, T. Aritsuki, R. S. O, and M. Nagase, *Appl. Phys. Express* **8**, 036602 (2015).
- 25) M. Kitaoka, T. Nagahara, K. Nakamura, T. Aritsuki, K. Takashima, Y. Ohno, and M. Nagase, *Jpn. J. Appl. Phys.* **56**, 085102 (2017).
- 26) F. Fromm, M. H. O. Jr, A. M. Sanchez, M. Hundhausen, J. M. J. Lopes, H. Riechert, L. Wirtz, and Seyller, *New J. Phys.* **15**, 043031 (2013).
- 27) M. Nagase, H. Hibino, H. Kageshima, and H. Yamaguchi, *Appl. Phys. Express* **6**, 055101 (2013).
- 28) A. Politano, G. Chiarello, C. Spinella, *Mater. Sci. Semicond. Process.* **65**, 88 (2017).
- 29) V. Ryzhii, M. Ryzii, V. Mitin, M. S. Shur, and T. Otsuji, *Phys. Rev. Appl.* **16**, 014001 (2021).
- 30) A. K. Dutta, *Phys. Rev.* **90**, 187 (1953).
- 31) K. M. M. Habib, S. Ge, M. Neupane, and R. K. Lake, *Appl. Phys. Lett.* **103**, 243114 (2013).

Figure Captions

Fig. 1. (a) Top and (b) side views of the stacked graphene diode. One sample was rotated 60° to align their crystallographic orientations. A gold-coated contact probe was placed at the four corners of each sample. (c) The device with two samples fixed using acrylic molds.

Fig. 2. Equivalent circuit of the stacked graphene diode, where R_j and R_a are the resistance and access resistance of the graphene junction, respectively.

Fig. 3. (a) 2-terminal $I-V_b$ and (b) 4-terminal $I-V_j$ characteristics of the device and graphene junction, respectively. Junction resistance (R_j) was high (5.9 k Ω) in the low-voltage applied region and low (0.2 k Ω) in the high-voltage applied region ($|V_b| = 90$ V).

Fig. 4. $I(t)-V_j(t)$ characteristics of the stacked graphene junction are plotted on a current-voltage graph.

Fig. 5. Variations in (a) V_j and (b) I at high ($V_b = 90$ V) and low ($V_b = 10$ V) voltages over time.

Fig. 6. (a) Conductance-junction voltage characteristics of the graphene junction. Initial conductance (G_{j0}) was 0.11 mS. (b) Conductance-junction voltage ($|V_j|$) characteristics of 3-junction devices in a double logarithmic graph. Devices 1–3 are same structure junction devices. Blue line shows the average value (0.13 mS) for 3 devices G_{j0} , and orange line was indicated by eq. (2), based on average values (Table 1) of S_0 and a .

Table 1. Each parameter is the absolute value characterized for the three devices, respectively. On/off is the ratio of the final state conductance to G_{j0} (mS), the initial state conductance. $|V_{j\text{-max}}|$ (V) is the maximum junction voltage. S_0 and a are plotted using the orange line in Fig. 6 (b).

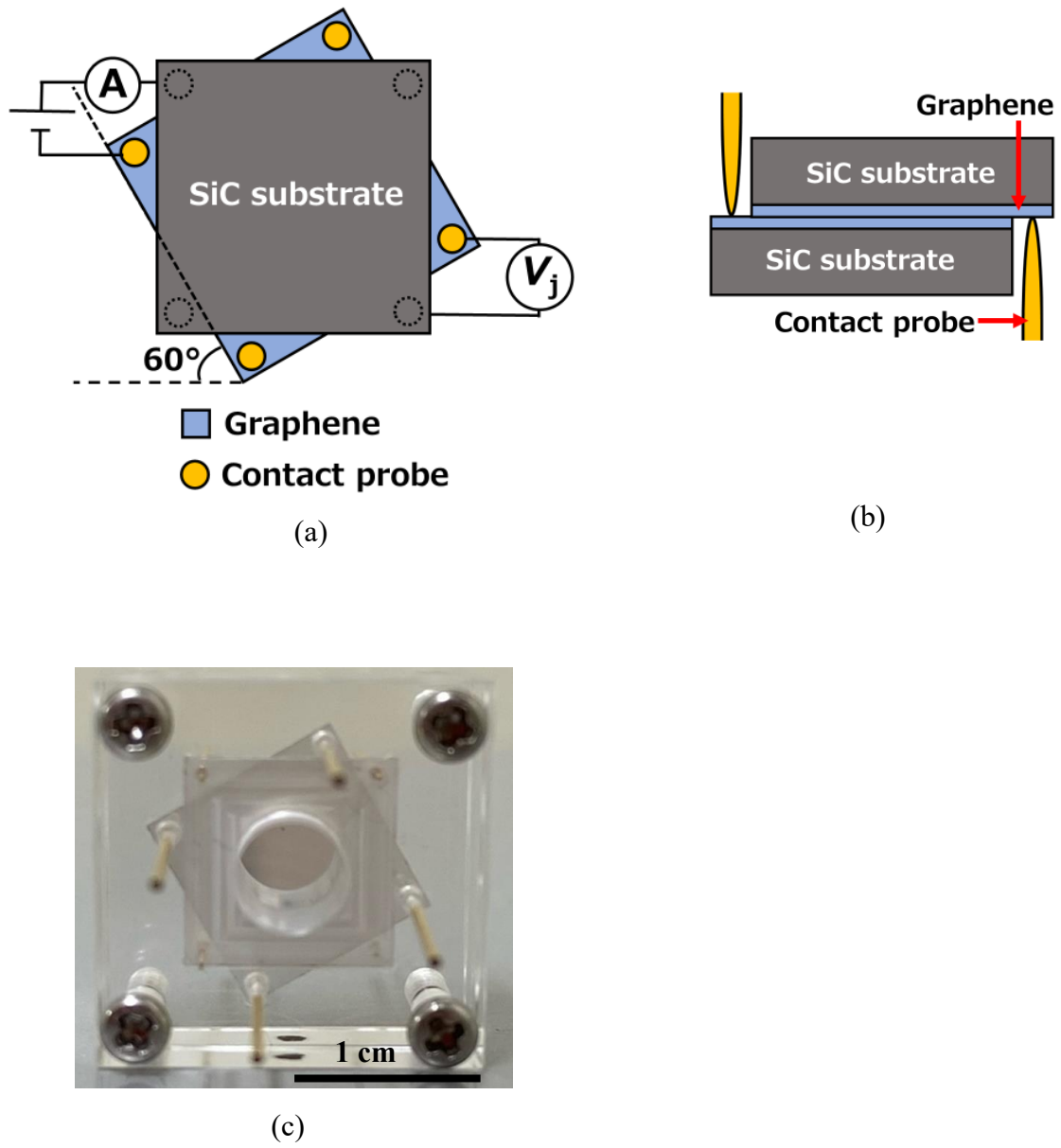


Fig. 1.

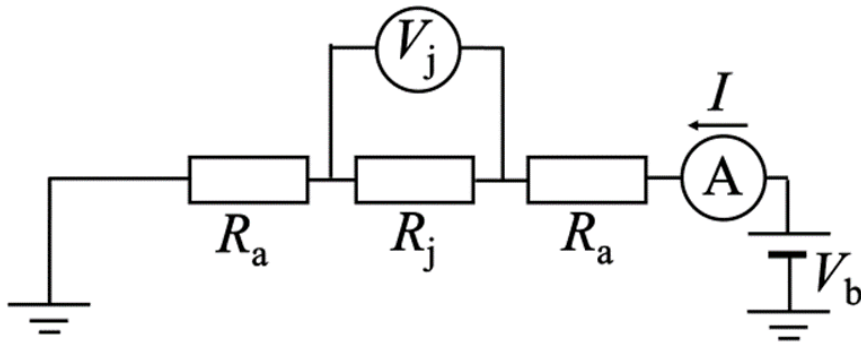


Fig. 2.

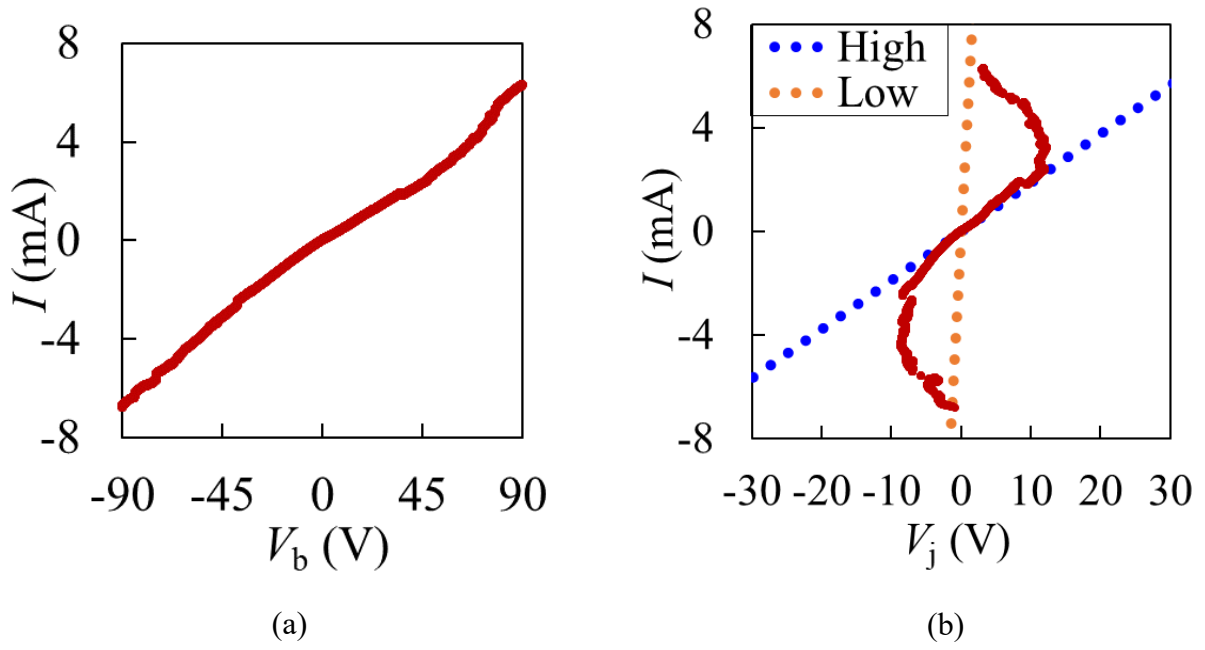


Fig. 3.

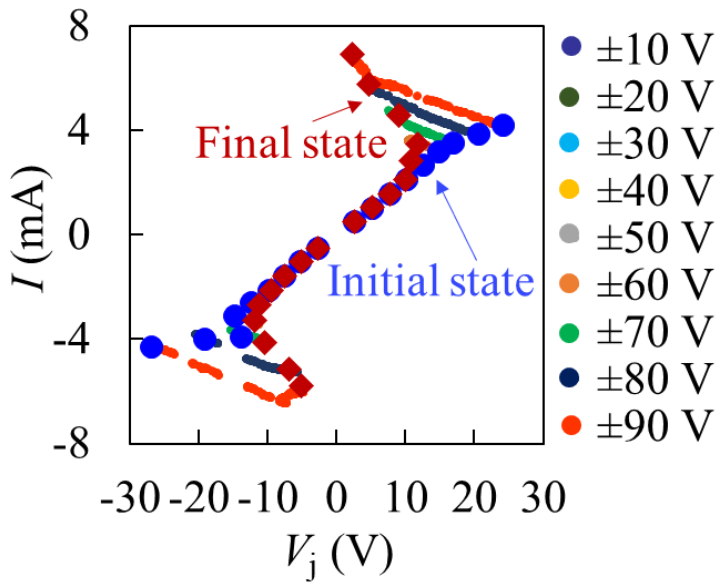
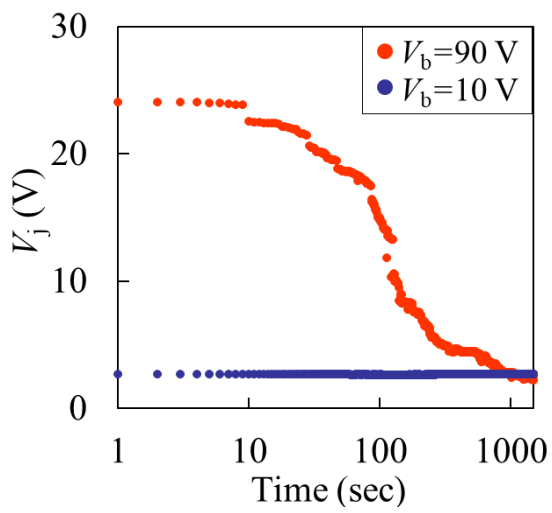
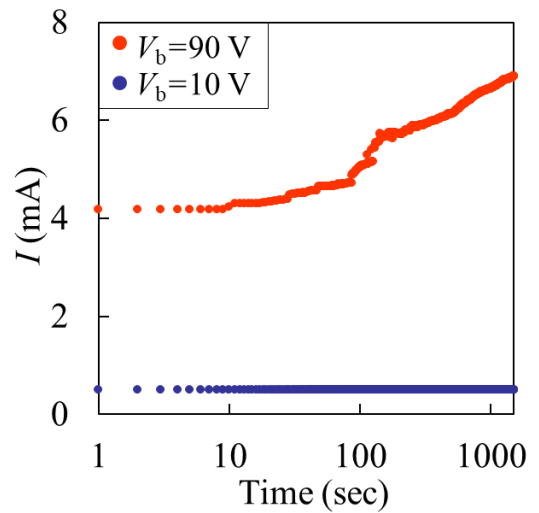


Fig. 4.



(a)



(b)

Fig. 5.

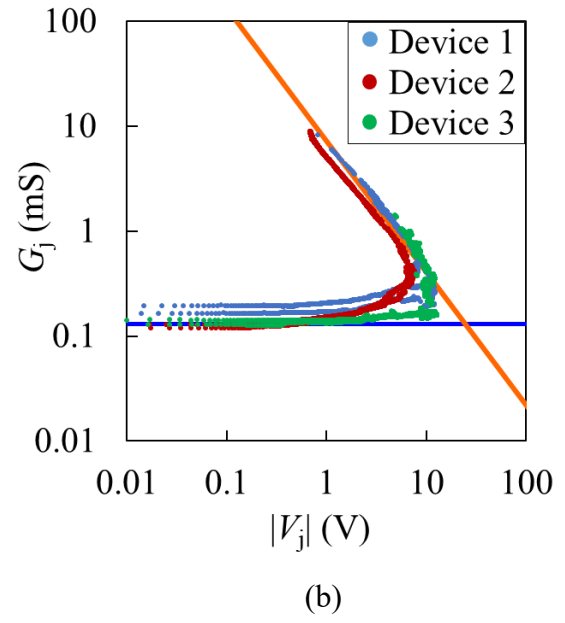
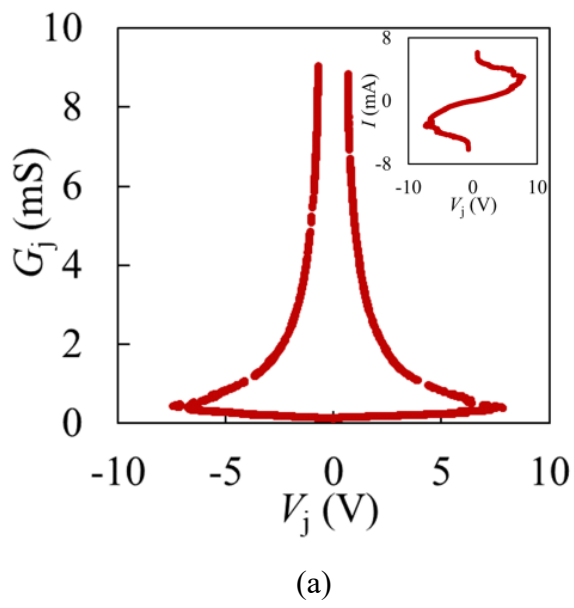


Fig. 6.

Table 1.

	on-off	$ V_{j\text{-max}} $ (V)	G_{j_0} (mS)	S_0	a
Device 1	29.8	10.5	0.17	0.0083	1.24
Device 2	75.9	7.65	0.11	0.0053	1.24
Device 3	11.1	12.7	0.11	0.0109	1.30
average	38.9	10.3	0.13	0.0082	1.26